Plasmon-Modulated Photoluminescence of Individual Gold Nanostructures

Hailong Hu,[†,⊥] Huigao Duan,[‡,§,⊥] Joel K. W. Yang,[‡,*] and Ze Xiang Shen[†,*]

[†]School of Physical and Mathematical Sciences, Nanyang Technological University, 21 Nanyang Link, 637371 Singapore, [‡]Institute of Materials Research and Engineering, A*STAR (Agency for Science, Technology and Research), 3 Research Link, 117602 Singapore, and [§]Key Laboratory for Micro-Nano Optoelectronic Devices of Ministry of Education, Hunan University, Changsha 410082, China. [⊥]These authors contributed equally to this work.

ABSTRACT In this work, we performed a systematic study on the photoluminescence and scattering spectra of individual gold nanostructures that were lithographically defined. We identify the role of plasmons in photoluminescence as modulating the energy transfer between excited electrons and emitted photons. By comparing photoluminescence spectra with scattering spectra, we observed that the photoluminescence of individual gold nanostructures showed the same dependencies on shape, size, and plasmon coupling as the particle plasmon resonances. Our results provide conclusive evidence that the photoluminescence in gold nanostructures indeed occurs *via* radiative damping of plasmon resonances driven by excited electrons in the metal itself. Moreover, we provide new insight on the underlying mechanism based on our analysis of a reproducible blue shift of the photoluminescence peak (relative to the scattering peak) and observation of an incomplete depolarization of the photoluminescence.

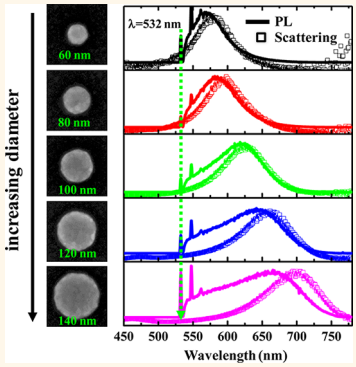

KEYWORDS: photoluminescence · plasmons · excited electrons · dark-field scattering · gold nanostructures

In addition to producing strong localized electric fields,[1−3] resonant plasmons in noble metal nanostructures are also responsible for the absorption of photons to create excited or hot electrons in the metal.[4−6] These properties are of great importance in light−matter interactions, in particular, to enhance the spontaneous emission of semiconductor nanomaterials[7] or molecules.[8] Interestingly, the inverse process, namely, of generating photons from non-equilibrium electrons in metal nanostructures themselves, can be facilitated by resonant plasmons, as well. The efficacy of this resonant effect has been observed in the photoluminescence (PL) of gold nanoparticles being several orders of magnitude larger than in the bulk film.[9−12] Consequently, PL in gold nanoparticles has been ascribed to the radiative damping of particle plasmons generated by the recombination of sp band electrons and excited d band holes.[10] However, some doubt remains in the involvement of plasmons in the PL process,[12−15] and an agreement in a mechanism for the PL process in nanostructures is lacking.

In this work, we performed a comprehensive study correlating PL with dark-field scattering spectra of individual lithographically defined Au nanostructures of different geometries. Realizing that the effect of plasmon coupling between nanostructures on PL has yet to be investigated, we looked also at dimers with varying gap sizes, which have been demonstrated to tune the plasmon resonance from the visible to the infrared wavelengths.[16−18] Detailed analysis on the PL peaks, absolute intensities, and line widths of the gold nanostructures was done. We observed that the PL of Au nanostructures shows a close correlation for shape, size, and coupling dependences as do their plasmon resonances. We observed a universal blue shift in the PL peak position with respect to the plasmon resonance and a preference for PL emission in the same polarization as that of the incident laser. These results provide conclusive evidence that incident photons absorbed by individual Au nanoparticle/dimer form excited electrons that result in PL through the radiative damping of bright plasmon resonance modes. Our results give insight into the details of the PL process and

* Address correspondence to zexiang@ntu.edu.sg, yangkwj@imre.a-star.edu.sg.

Received for review August 26, 2012 and accepted October 16, 2012.

Published online October 16, 2012
10.1021/nn3039066

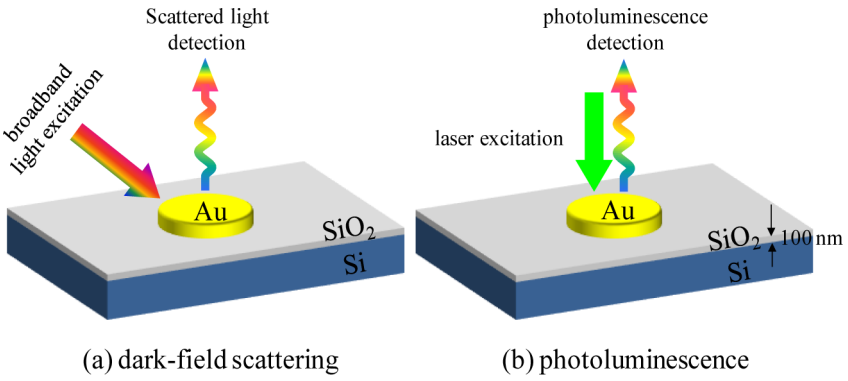

Figure 1. Schematics illustrating the optical excitation and collection setup for dark-field scattering and photoluminescence. Measurements were done for gold nanostructures fabricated by electron-beam lithography on 100 nm thick SiO_2 dielectric on Si substrates. (a) In dark-field scattering, a broadband light introduced at glancing angles is elastically scattered and subsequently collected by an objective lens. The most intense scattering occurs at the plasmon resonance condition of the nanostructure. (b) In photoluminescence, a continuous wave (CW) excitation laser with the wavelength of 532 nm normal to the substrate was introduced and induces inelastic processes within the nanostructures. The Stokes-shifted photoluminescence from the nanostructures was collected.

should also remove any doubts of the role of plasmons in PL.

RESULTS AND DISCUSSION

The plasmon resonances of Au nanostructures were characterized by dark-field microscopy prior to the PL measurements. Figure 1 shows the schematic diagrams of dark-field (DF) scattering (1a) and photoluminescence (1b) measurements. In dark-field scattering, the Au nanostructure was illuminated with a broadband white light at glancing incidence, as indicated in Figure 1a. The elastically scattered light, as marked by a colorful wavy arrow, was collected by an objective positioned above the sample. In the photoluminescence setup, a linearly polarized green laser (λ = 532 nm) excited the photoluminescence of Au nanostructures at normal incidence. In our experiments, the photoluminescence and scattering spectra were recorded using the same setup with the only difference being the excitation source and illumination angles. Details about the optical measurements of scattering and photoluminescence spectra and their analyses are in the Methods section.

To systematically investigate the photoluminescence of Au nanostructures and the role of surface plasmons, we fabricated a set of Au nanostructures with different shapes, sizes, and gap sizes by electron-beam lithography (EBL). The thickness of the Au nanostructure was 30 nm with a 1 nm Cr adhesion layer. A gold film was also fabricated on the same sample as a reference for PL measurement (see Methods for fabrication details).

Figure 2 shows the dark-field scattering and PL results obtained from single Au nanoparticles with three different geometries. Figure 2a shows SEM images of the nanodisk, nanotriangle, and nanorod. With the help of registration marks (Figure S1 in Supporting Information), we were able to precisely collect the scattering and PL spectra from the exact Au nanostructures as imaged in the SEM. Both the white light source and excitation laser were polarized along the horizontal direction. In Figure 2b, we see that these three types of nanoparticles in scattering spectra show clear plasmon resonances with peaks at 596 nm (disk), 634 nm (triangle), and 661 nm (rod). When excited by a 532 nm laser, these nanoparticles showed an obvious shape-dependent PL with peaks appearing at 588 (disk), 621 (triangle), and 653 nm (rod), as illustrated in Figure 2c.

Close correlations in peak positions and spectral line widths between the PL and scattering spectra, as shown in Figure 2d, suggest the dominant role of plasmon resonances in the generation of photoluminescence. The shift of plasmon resonances due to changing nanostructure shape was closely tracked in the resulting PL spectra. It is therefore unlikely that photoluminescence arose solely from the direct recombination of sp electrons and d holes,[14,19,20] as such a direct recombination would result in a spectrum that was shape-independent and depended only on material and temperature. On the other hand, the broad peaks in plasmon resonances as measured by their line widths are known to originate from photon emission (radiative damping) and absorption (dephasing or nonradiative damping).[21,22] Hence the match in line width between PL and scattering from these nanostructures suggests that the PL process indeed occurred *via* plasmon generation, hence sharing the same damping mechanism.

We observed that the photoluminescence peaks were consistently blue-shifted (~10 nm in wavelength) with respect to the scattering peaks, as illustrated in Figure 2d. We have carefully investigated the origin of this blue shift to ensure that it is reproducible and not due to the effect of varying excitation collection angles[23] in dark-field microscopy. We observed no

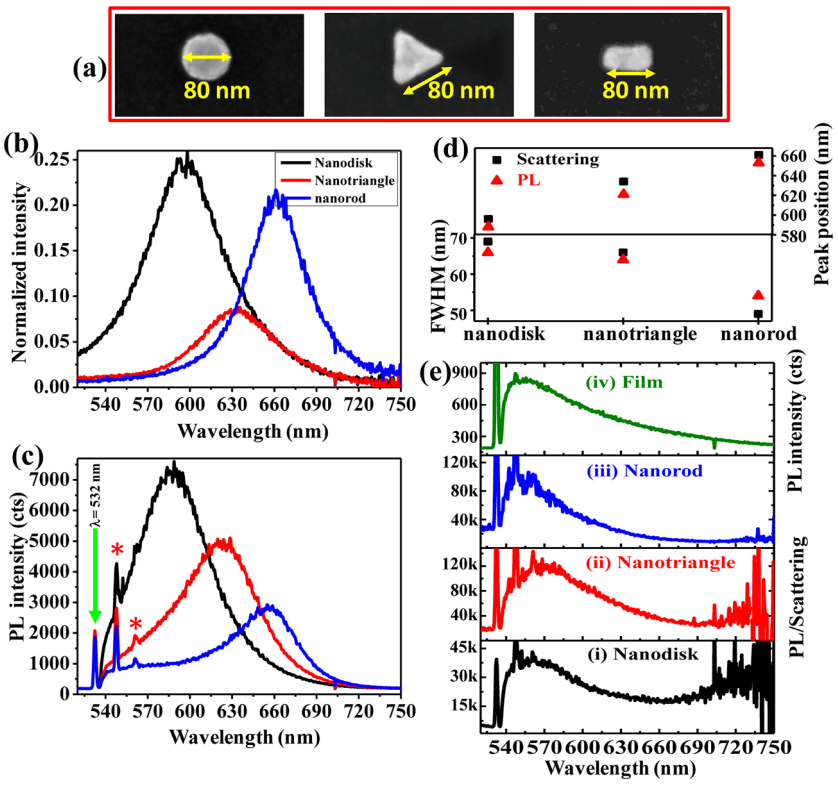

Figure 2. Shape-dependent photoluminescence (PL) of single Au nanoparticles. (a) SEM images of the single Au nanodisk, nanotriangle, and nanorod used in the measurements. (b,c) Corresponding dark-field scattering spectra and PL spectra of these particles, respectively, color-coded to the particular nanostructure shape. The excitation wavelength for PL was 532 nm. The green arrow in (c) indicates the Rayleigh scattering of the laser, while the sharp peaks marked by the red stars belong to the first- and second-order Raman scattering of the SiO_2/Si substrate. (d) Plot of peak position and fwhm for different geometries showing the close correlation between PL (red) and scattering (black) spectra in (c) and (b). (e) i−iii: PL/scattering ratio of the three nanoparticles, showing similar profiles and trends as the PL spectrum of an unpatterned Au film (iv), suggesting a link between film PL and PL/scattering ratio of nanostructures as described in the text.

dependence on collection angle in scattering spectra collected using objective lenses with different numerical apertures (NA = 0.5, 0.75 and 0.9; see Figure S2). We also show that the blue shift in PL relative to scattering spectra was systematically larger than the slight shifts that could result from differences between absorption and scattering cross sections, which are less than 8 nm, as shown in Figure S3. The following spectral analysis offers a possible explanation to this blue shift. Note that the relative peak intensities for PL of $I_{disk} > I_{triangle} > I_{rod}$ are different from those in scattering where $I_{disk} > I_{rod} > I_{triangle}$. However, it is surprising that the ratios of PL to scattering spectra exhibit similar profiles for all three nanostructures, as shown in Figure 2e(i−iii). More interestingly, those profiles closely resemble the photoluminescence spectrum of bulk Au film, as shown in Figure 2e(iv), which is known to arise from the thermalization of photoexcited non-equilibrium electrons in the absence of particle plasmons.[13,19] The resemblance can be rationalized by considering that this "material-dependent" thermalization process occurs in nanostructures in the same way as in an unpatterned film, presumably before the electrons excite particle plasmons. Thus, taking the ratio of PL to scattering spectra intuitively normalizes out the contribution of the plasmon antenna scattering strength from the PL spectra and provides a distribution of the non-equilibrium electrons available for the excitation of plasmons that lead to PL emission. Thus, this admittedly simple analysis suggests that the blue shift of the observed PL could be due to the higher availability of excited electrons closer to the initial energy of the laser excitation. To validate this hypothesis, further solid-state theoretical calculations and experiments are needed.

We now present another important plasmon effect on PL, that is, the size of nanostructures. Scattering and PL measurements were done on single Au nanodisks with diameters ranging from 60 to 140 nm, as shown in Figure 3a. The corresponding scattering and PL spectra are illustrated in Figure 3b,c, respectively. As seen in Figure 3b, increasing the diameter of the nanodisks, both intensified and red-shifted the plasmon resonance, as expected. The corresponding PL spectra are displayed in Figure 3c, showing similar size dependence with scattering spectra. The blue shift of PL peaks was also reproducibly observed here as it was in Figure 2. Simulation results for the corresponding structures are shown in Figure 3d, with excellent agreement shown in Figure 3e together with the blue shift of the PL peaks.

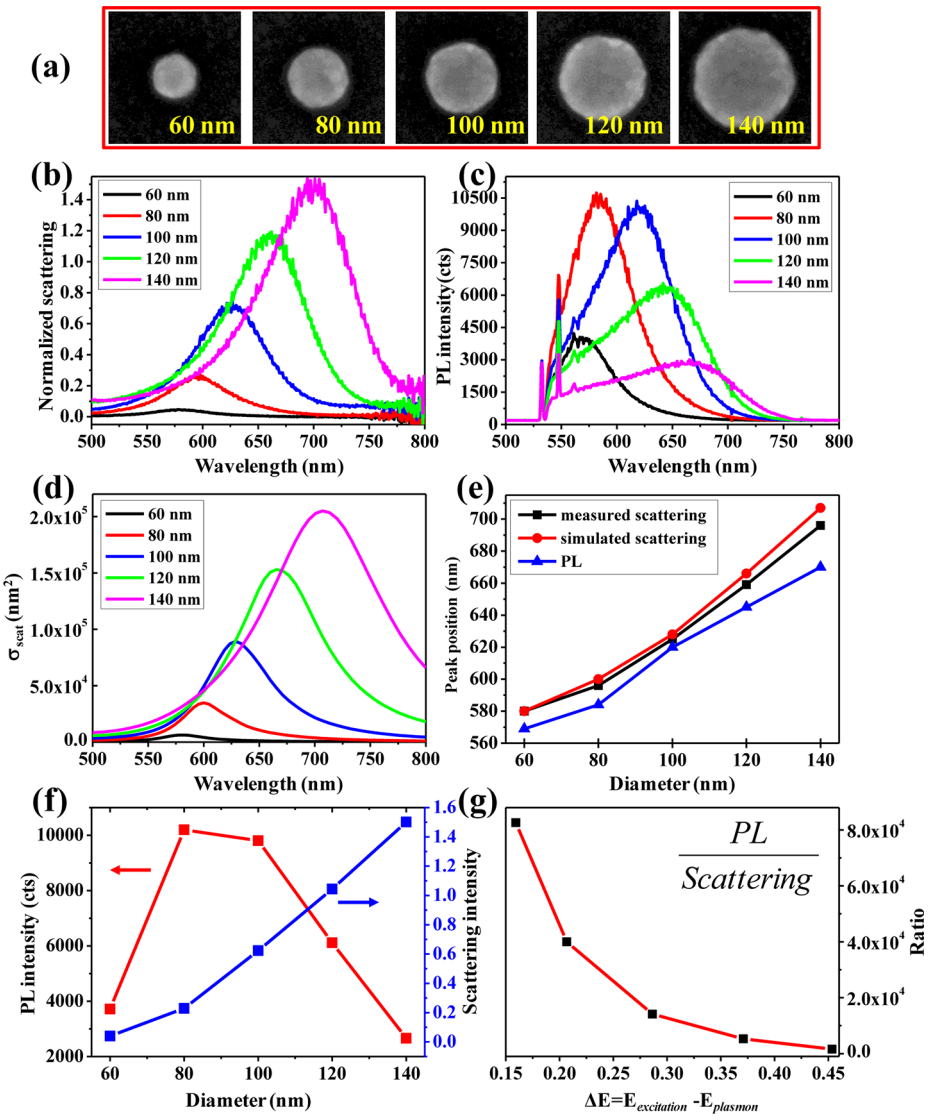

Figure 3. PL of Au nanodisks with different sizes to demonstrate dependence of PL intensity on energy mismatch between excitation laser and plasmon resonance. (a) SEM images of the single Au nanodisks with different diameters from 60 to 140 nm. (b,c) Dark-field scattering and PL spectra of the particles in (a), showing size dependence. (d) Numerical simulation of scattering spectra using finite-difference time domain (FDTD), closely matching experimental results. (e) Peak positions of measured (black), simulated (red) scattering, and PL (blue) spectra, indicating the correlation between PL and plasmon resonance. (f) Scattering (blue curve) and PL (red curve) intensities as a function of the particle size. (g) Plot of the PL/scattering ratio at the PL peak position of each particle as a function of the energy mismatch (ΔE) between excitation laser and the plasmon resonance energies.

Figure 3f shows the different trends in the PL and scattering peak intensities. The absolute PL intensity was highest for the 80 nm nanodisk, while the scattering intensities showed a monotonically increasing trend. This decrease in PL for larger nanodisks is rather surprising for two reasons: (1) the larger nanodisks are better scatterers, and so should more strongly reradiate the absorbed light through PL; and (2) they absorb more of the laser light due to their larger absorption cross sections (see simulation results in Figure S3), which should also provide more energy for PL. The reason for the decrease in PL can be explained by considering the energy mismatch between the excitation laser and the PL peak. With larger nanodisks, the PL peak occurs at longer wavelengths where there are fewer non-equilibrium electrons to excite plasmons. To illustrate this point, we first normalized the PL intensity by scattering intensity taken at the different PL peak energies, similar to what was done in Figure 2e, and obtained the plot shown in Figure 3g. When plotted as a function of the energy difference between the excitation and PL peak energy, ΔE, we indeed observe that the amount of excited plasmons decreases monotonically when the energy match between excitation and plasmon resonance becomes poorer. It is satisfying to see a connection between this trend and that of the PL spectrum in Figure 2e. The resemblance simply reflects the fact that the non-equilibrium electrons are

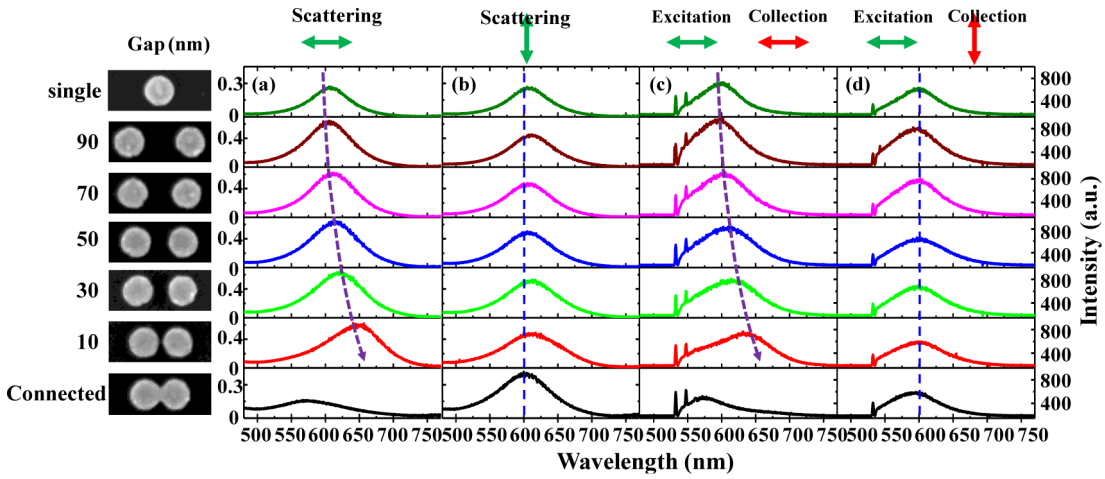

Figure 4. PL and scattering spectra of coupled 80 nm Au nanodisks with varied gap size (shown in the SEM images). (a) Scattering spectra of the structures at horizontally polarized white light excitation, showing a consistent red shift of the plasmon peak with decreasing gap size and the appearance of a high-energy plasmon peak in the connected structure. (b) Scattering spectra of the structures at vertically polarized excitation, with no significant energy shift of the peaks when changing the gap size. (c) PL spectra of the structures obtained with both horizontal excitation and collection polarization, in which the peaks show exactly the same trend as these in scattering spectra with horizontal excitation (a). (d) PL spectra of the structures obtained with horizontal excitation but vertical collection polarization, in which no peak shift was found, same as the observations in scattering spectra with vertical excitation (b). Note that PL intensities in (c) and (d) are shown at the same scale. The green double arrows indicate the excitation polarization directions, while the red double arrows indicate the collection polarization directions.

more highly populated at energies closer to their initial excited states, that is, at small ΔE, hence leading to higher PL intensities as there are more available non-equilibrium electrons to excite plasmons.

A key feature of plasmons is their coupling behavior in closely spaced nanostructures, as manifested by shifts in the resonances as the gap size between the nanostructures is varied.[24] Though plasmon coupling effects in two-photon photoluminescence (TPPL) have been demonstrated,[25,26] to the best of our knowledge, the following is the first systematic study of the effect of plasmon coupling on single-photon luminescence. A systematic investigation on the PL of coupled plasmonic structures should provide us with further insight into how it modulates the PL process.

Figure 4 shows results of scattering and PL from an individual and several coupled 80 nm gold nanodisks with gap sizes from 0 to 90 nm. For comparison, we first show the scattering spectra of these structures in Figure 4a (horizontal excitation) and 4b (vertical excitation), from which the trends for the different resonant modes as reported in previous studies are similarly observed.[3,27,28] In brief, in the horizontally polarized excitation, the dipolar bright mode consistently red shifts when decreasing the gap size, which increases the capacitance of the facing edges of the disks that get cyclically charged. The peak at ~550 nm in the connected structure corresponds to a high-energy quadrupolar mode (see Figure S5). Though a low-energy charge-transfer mode is supported in the connected structure, it was beyond the measurement range of our detectors. In the vertical excitation, the resonant plasmon mode corresponding to charge oscillations along the direction of the excitation leaves the facing edges of the disks uncharged, hence its independence to gap size variation.

The unpolarized collection of the PL spectrum for the dimer was much broader than that of the single nanodisk (see Figure S4). In order to identify the origin of PL in coupling system, we placed a linear analyzer, parallel or perpendicular to the laser excitation polarization, in the collection path. Figure 4c,d shows the corresponding polarized PL spectra of the structures with fixed horizontal polarized laser excitation but with different collection polarizations. From Figure 4c, it can be seen that the PL spectra collected from dimers along the horizontal polarization are distinct from that of the single nanodisk. Rather, they show the same trend as their corresponding scattering spectra in Figure 4a. Hence, the PL along the horizontal direction originated from the coupled bright dipolar modes. In contrast, no energy shift was found in the PL spectra collected in the vertical polarization, resembling the corresponding scattering spectra (Figure 4b), as governed by the transverse plasmon resonances. Though the excitation was along the horizontal direction, PL emissions polarized in the orthogonal direction have previously been reported[29−31] and are attributed to the dephasing or depolarization of the plasmon and electron scattering events, as discussed later. This set of experiments demonstrates for the first time that PL arising from plasmons in coupled structures follows the resonance shifts of the plasmons. Almost trivially, an argument that PL was solely due to electronic processes within a given nanostructure would be incorrect, as such processes would be unperturbed by

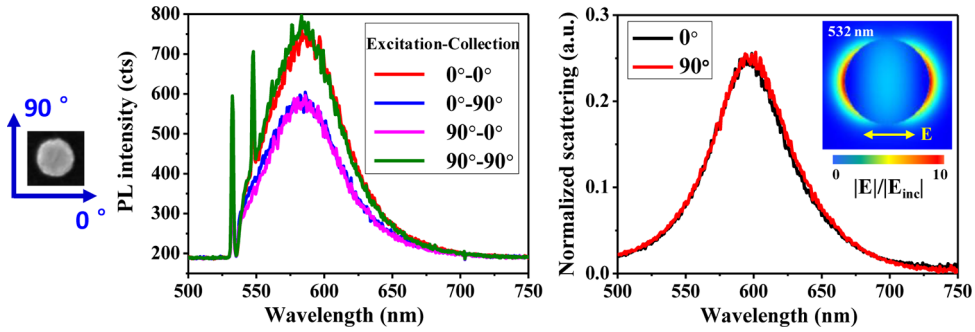

Figure 5. Excitation polarization dependence of the photoluminescence spectra from a single 80 nm diameter symmetric Au nanodisk, as shown by the SEM image. The nanodisk shows incomplete depolarization where PL emission occurs preferentially in the same polarization as the excitation (*i.e.*, red and green lines have higher intensities than blue and pink lines). The excitation and collection polarization angles relative to the structure are indicated by the blue arrows. In contrast, the right panel shows near identical scattering spectra of the nanodisks for two orthogonal white light polarizations. Inset shows the simulated electric field distribution under 532 nm laser excitation.

the presence of a nearby nanostructure. Rather, the results here provide further evidence that PL is a consequence of the radiation damping of plasmon resonances, with modes that are supported across multiple nanostructures.

To obtain further insight of the depolarization process of the incident photons caused by the thermalization of photoexcited electrons, we investigated the excitation and collection polarization dependence of the PL spectra in terms of peak intensities. A symmetric nanodisk was selected as an example for this study. Two different excitation polarizations (0° and 90°) were used, and the PL was collected also in two different configurations: 0° and 90° direction. From Figure 5, we see that, under parallel (0−0° and 90−90°) or orthogonal (0−90° and 90−0°) configuration, the almost identical polarized PL spectra indicate independence on the excitation polarization, which confirms that the incident photons lost their polarization during the photoluminescence process.

The complete depolarization of photoexcited electrons due to fast thermalization in PL is well-known in single Au nanorods[11,12] and colloidal Au nanospheres,[13] accounting for the independence of PL on polarization of the laser excitation. In other words, once a photon is absorbed, all "memory" of the polarization of the photon is lost. However, as demonstrated using the symmetric nanodisk in Figure 5, we surprisingly found that the emitted light (through radiative damping of plasmons) had a tendency (~25% higher in this particle) to be polarized in the same direction as the incident light. This preferential PL from the same excitation polarization suggests incomplete depolarization of the incident light in the processes prior to plasmon excitation and radiative damping. To avoid the possibility of preferential scattering in any particular direction, we measured scattering spectra at the two orthogonal polarization directions and obtained identical scattering intensities, as shown on the right panel in Figure 5.

One hypothesis for this incomplete depolarization is that the non-equilibrium electrons are not uniformly distributed within the disk but are instead localized in the regions of the highest laser field intensities. From the simulated electric field distribution in the inset of Figure 5, the continuous wave (CW) green laser (532 nm) creates strong localized electric fields along the opposite edges of the disk along the direction of the laser polarization. These are the edges where electrons are preferentially photoexcited due to the stronger electric fields present. Given that the disks are larger than the electron mean free path of ~50 nm,[32] the excited electrons could remain non-uniformly distributed within the disk even after thermalization. Now, as we have learned from electron energy loss spectroscopy (EELS),[24,33,34] the position of the electron beam determines the plasmon resonance modes that are excited, with modes having stronger electric fields in the path of the beam being favorably excited. Analogously in PL, non-equilibrium electrons would preferentially excite plasmons that have a high electric field distribution right where these electrons are localized. In this particular case, the favored plasmon resonance mode would have a similar field distribution as that shown in the inset of Figure 5, which is along the polarization of the laser. Hence the incomplete depolarization arises due to the non-uniform distribution of non-equilibrium electrons in the disk.

To provide a visual picture for the plasmon-modulated PL of gold nanostructures, a simple mechanism diagram is given in Figure 6, in which the whole PL process is described by four steps, as indicated by the numbers in Figure 6a.

(1) Plasmon-enhanced excitation of electrons from the ground state to the photoexcited states with energy of 2.33 eV by 532 nm laser.

(2) Excited electrons thermalize to form a population distribution in the conduction band due to scattering, leading to a broad and inhomogeneous energy profile of non-equilibrium electrons. This distribution is the

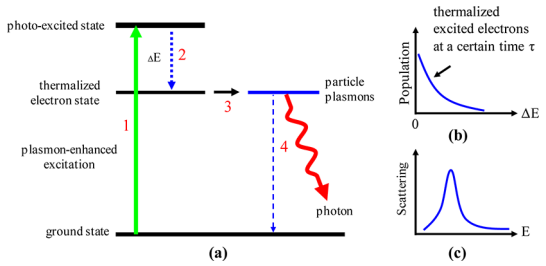

Figure 6. Proposed mechanism of plasmon-modulated PL of gold nanostructures. (a) Schematic diagram of a mechanism to qualitatively understand the PL of Au nanostructures. The whole process includes four steps: (1) plasmon-enhanced excitation of electrons shown as the green arrow; (2) thermalization of excited electrons, shown by a blue dashed arrow; (3) excitation of particle plasmons by non-equilibrieum electrons shown by the black arrow; (4) radiation damping of plasmon into photon, shown by the red wavy arrow. (b) Population distribution of thermalized hot electrons before the formation of surface plasmon. The probabilities for the forming plasmon resonance and radiative damping can be represented by the dark-field scattering spectrum in (c).

reason for the blue shift of PL spectrum with respect to plasmon resonance in scattering. The population of electrons at a certain energy state is a function of the energy difference (ΔE) relative to the initial state, as shown in Figure 6b, with larger ΔE having a lower population, as determined by the excited electron dynamics[29] and also manifested in the PL spectra from Au film.

(3) Thermalized electrons excite particle plasmon resonance. Resonant plasmons provide a large local density of optical states (DOS) that increases the decay rate of the excited electrons,[35,36] suggesting that excited electrons have a higher probability of exciting plasmons, in accordance to Fermi's golden rule. This additional path made available to the electrons competes with the direct recombination of these electrons with holes, thus modulating the PL over that of the bulk metal.

(4) Radiative damping of particle plasmons into photons, as shown by the red wavy arrow.

Using this model, we can intuitively estimate the PL spectra by two key processes:

$$\text{PL} \sim \text{population profile of thermalized electrons} \times \text{DOS}$$

where the population profile of thermalized electrons that resembles the PL spectrum from the gold film (as schematically shown in Figure 6b) provides a broadband background[37] while the DOS, which is represented by the scattering spectrum (as schematically shown by Figure 6c), determines the optical environment for the resonant decay of the thermalized electrons. This understanding suggests that plasmons are also excited most probably when (1) a high population of non-equilibrium electrons exists in the metal and (2) these electrons are localized where the density of optical states for the plasmons is highest. With this simple formula, we can explain our observations of the blue shift of PL spectra and energy mismatch (ΔE) effect on the intensity of PL in Figures 2 and 3.

CONCLUSIONS

In conclusion, we presented a systematic study on photoluminescence (PL) of individual Au nanostructures, showing that the PL peak position can be modulated by their plasmon resonances. We show dependence of PL on the shape and size of single Au nanostructures and for the first time demonstrate PL from plasmon-coupled nanostructures. We report the observation of an incomplete depolarization of PL and hypothesize that it results from an inhomogeneous distribution of non-equilibrium electrons within the nanostructures. A simple mechanism was proposed to illustrate that PL results from the excitation of plasmon resonances by non-equilibrium electrons. Our results and analysis provide insights into processes that occur in PL of gold nanostructures that have implications also in cathodoluminescence and in the generation of plasmons in tunnel junctions *via* hot electrons.

METHODS

Fabrication. PMMA resist (950K molecular weight, 1.67% in anisole) from MicroChem Corp. was spin-coated at 3k rpm to be ~80 nm on SiO_2/Si substrates. The thickness of SiO_2 was 100 nm. We chose silicon as the substrates as doing so avoids charging effects during the electron-beam lithography (EBL) process, while 100 nm SiO_2 was used as a spacer layer to reduce plasmon damping caused by the silicon substrate. After spin-coating, the substrates were baked on a hot plate at 180 °C for 90 s. EBL was done with an Elionix ELS-7000 system with an accelerating voltage of 100 kV and a beam current of 50 pA. Optimized dose was used to obtain the structures we designed for the measurements. After exposure, the samples were developed with 1:3 MIBK/IPA developer at low temperature (−15 °C) for 30 s and then were directly blown dry using with a steady stream of N_2. Low-temperature development of PMMA provides higher contrast and pattern resolution.[1] Metal deposition was performed using an electron-beam evaporator (Explorer Coating System, Denton Vacuum). A 30 nm Au layer was deposited with 1 nm Cr adhesion layer. The working pressure during the evaporation was $<5 \times 10^{-6}$ Torr. The temperature of the sample chamber was kept at 20 °C during the entire evaporation process, with the sample holder rotating at a rate of 50 rpm to ensure the uniformity of deposition. Lift-off was done by immersing samples in *N*-methylpyrrolidone (NMP) solvent at an elevated temperature of 70 °C.

Optical Measurements. Dark-field scattering and PL measurements of an individual Au nanostructure were performed on a WITec CRM200 confocal Raman microscopy system. The scattering and PL spectra were dispersed by 150 lines/mm grating and detected using a TE-cooled CCD (Andor DV 401-BV-351). High-resolution spectrograph (0.55 nm/pixel) allows peak positions of scattering and PL to be accurate within ±1 nm.

For dark-field scattering measurement, a halogen lamp (15 V, 150 W, 3150 K) served as the white source and illuminated the sample *via* a dark-field objective lens (100×, NA = 0.75), which was also used to collect the scattering light. The integration time for scattering spectra was set as 20 s. In our experiments, for all of the scattering spectra presented, contributions from substrate scattering were excluded. Results were normalized with

the light source spectrum and the response curve of the entire optical system. The details of calculation are described in the formula below:

$$I_{scat}(\lambda) = \frac{I_{particle} - I_{sub}}{I_{halogen} - I_{dark}}$$

where $I_{scat}(\lambda)$ is the real scattering spectrum of a single nanoparticle; $I_{particle}$ and I_{sub} are the original scattering spectra collected from the nanoparticle and adjacent substrate without nanoparticle, respectively. $I_{halogen}$ and I_{dark} are the spectrum of the halogen light source and the background count of our system, respectively. Polarization-dependent scattering spectra were achieved using the same setup as used in the measurement of photoluminescence.

For PL measurement, a linearly polarized green laser with the wavelength of 532 nm was selected as the excitation source and focused on the single Au nanoparticle *via* a Zeiss Epiplan objective lens (100×, NA = 0.75, HD). The laser power was set as 50 μW to excite the PL. All PL spectra were obtained with an integration time of 20 s. A piezoelectric stage was used to approach the maximum luminescence intensity. The luminescence spectra under parallel and perpendicular polarizations (0 and 90°) were achieved by manually rotating the sample. An analyzer was placed after the objective lens to record light polarized along the 0 or 90°.

To verify whether obtaining the PL spectra was a one-photon process, we investigated the PL intensity as a function of the excitation laser power, as shown in Figure S5. The results show that the PL intensity was linearly proportional to the laser power, suggesting one-photon luminescence, rather than two- or three-photon luminescence in which PL intensity was proportional to the square or cube of laser power.

FDTD Simulations. Theoretical scattering spectra for individual Au nanostructures were calculated by commercial 3D finite-difference time-domain (FDTD) Solutions 7.5 (Lumerical Solutions, Inc.). The Au nanostructure was modeled according to the size measured from SEM images. The influence of the Si substrate with a 100 nm SiO_2 layer was included to ensure the scattering signals were real. The complex dielectric constants for Au, SiO_2, and Si were from Johnson-Christy and Palik, respectively. The Cr adhesion was not included in the simulations for simplification. The mesh size used for the SiO_2/Si substrate region was 5 nm in the *z* direction and 1 nm in two in-plane directions. A fine mesh grid was added for the 0.5 nm Au nanostructure. Perfectly matched layer (PML) boundary condition was set for all three dimensions. Total field and scattering field source ranging from 400 to 800 nm directed along the *z*-axis was illuminated to simulate the absorption, scattering, and extinction spectra. The electric field distribution of the single 80 nm nanodisk excited by 532 nm light was simulated.

Conflict of Interest: The authors declare no competing financial interest.

Acknowledgment. This work was supported by the Agency for Science, Technology and Research (A*STAR) in Singapore. The work made use of the SERC nano Fabrication, Processing and Characterization (SnFPC) facilities in IMRE. H.D. thanks the sponsorship from National Science Foundation of China (Grant Nos. 11274107 and 61204109). The authors acknowledge H. Sun (NTU), Y. T. Chan (NUS), B. Ren (Xiamen University), and H. A. Atwater (Caltech) for fruitful discussions.

Supporting Information Available: More results are provided by the supporting Figures S1−S5. This material is available free of charge *via* the Internet at http://pubs.acs.org.

REFERENCES AND NOTES

1. Hao, E.; Schatz, G. C. Electromagnetic Fields around Silver Nanoparticles and Dimers. *J. Chem. Phys.* **2004**, *120*, 357–366.
2. Duan, H. G.; Hu, H. L.; Kumar, K.; Shen, Z. X.; Yang, J. K. W. Direct and Reliable Patterning of Plasmonic Nanostructures with Sub-10-nm Gaps. *ACS Nano* **2011**, *5*, 7593–7600.
3. Halas, N. J.; Lal, S.; Chang, W. S.; Link, S.; Nordlander, P. Plasmons in Strongly Coupled Metallic Nanostructures. *Chem. Rev.* **2011**, *111*, 3913–3961.
4. Knight, M. W.; Sobhani, H.; Nordlander, P.; Halas, N. J. Photodetection with Active Optical Antennas. *Science* **2011**, *332*, 702–704.
5. Mubeen, S.; Hernandez-Sosa, G.; Moses, D.; Lee, J.; Moskovits, M. Plasmonic Photosensitization of a Wide Band Gap Semiconductor: Converting Plasmons to Charge Carriers. *Nano Lett.* **2011**, *11*, 5548–5552.
6. Hentschel, M.; Utikal, T.; Giessen, H.; Lippitz, M. Quantitative Modeling of the Third Harmonic Emission Spectrum of Plasmonic Nanoantennas. *Nano Lett.* **2012**, *12*, 3778–3782.
7. Lee, J.; Govorov, A. O.; Dulka, J.; Kotov, N. A. Bioconjugates of CdTe Nanowires and Au Nanoparticles: Plasmon−Exciton Interactions, Luminescence Enhancement, and Collective Effects. *Nano Lett.* **2004**, *4*, 2323–2330.
8. Russell, K. J.; Liu, T.-L.; Cui, S.; Hu, E. L. Large Spontaneous Emission Enhancement in Plasmonic Nanocavities. *Nat. Photonics* **2012**, *6*, 459–462.
9. Mohamed, M. B.; Volkov, V.; Link, S.; El-Sayed, M. A. The 'Lightning' Gold Nanorods: Fluorescence Enhancement of over a Million Compared to the Gold Metal. *Chem. Phys. Lett.* **2000**, *317*, 517–523.
10. Dulkeith, E.; Niedereichholz, T.; Klar, T. A.; Feldmann, J.; von Plessen, G.; Gittins, D. I.; Mayya, K. S.; Caruso, F. Plasmon Emission in Photoexcited Gold Nanoparticles. *Phys. Rev. B* **2004**, *70*, 205424-4.
11. Yorulmaz, M.; Khatua, S.; Zijlstra, P.; Gaiduk, A.; Orrit, M. Luminescence Quantum Yield of Single Gold Nanorods. *Nano Lett.* **2012**, *12*, 4385–4391.
12. Tcherniak, A.; Dominguez-Medina, S.; Chang, W. S.; Swanglap, P.; Slaughter, L. S.; Landes, C. F.; Link, S. One-Photon Plasmon Luminescence and Its Application to Correlation Spectroscopy as a Probe for Rotational and Translational Dynamics of Gold Nanorods. *J. Phys. Chem. C* **2011**, *115*, 15938–15949.
13. Varnavski, O. P.; Goodson, T., III; Mohamed, M. B.; El-Sayed, M. A. Femtosecond Excitation Dynamics in Gold Nanospheres and Nanorods. *Phys. Rev. B* **2005**, *72*, 235405.
14. Beversluis, M. R.; Bouhelier, A.; Novotny, L. Continuum Generation from Single Gold Nanostructures through Near-Field Mediated Intraband Transitions. *Phys. Rev. B* **2003**, *68*, 11543-1.
15. Fang, Y.; Chang, W.-S.; Willingham, B.; Swanglap, P.; Dominguez-Medina, S.; Link, S. Plasmon Emission Quantum Yield of Single Gold Nanorods as a Function of Aspect Ratio. *ACS Nano* **2012**, *6*, 7177–7184.
16. Mock, J. J.; Barbic, M.; Smith, D. R.; Schultz, D. A.; Schultz, S. Shape Effects in Plasmon Resonance of Individual Colloidal Silver Nanoparticles. *J. Chem. Phys.* **2002**, *116*, 6755–6759.
17. Xia, Y. N.; Halas, N. J. Shape-Controlled Synthesis and Surface Plasmonic Properties of Metallic Nanostructures. *MRS Bull.* **2005**, *30*, 338–344.
18. Kelly, K. L.; Coronado, E.; Zhao, L. L.; Schatz, G. C. The Optical Properties of Metal Nanoparticles: The Influence of Size, Shape, and Dielectric Environment. *J. Phys. Chem. B* **2002**, *107*, 668–677.
19. Mooradia, A. Photoluminescence of Metals. *Phys. Rev. Lett.* **1969**, *22*, 185–187.
20. Boyd, G. T.; Yu, Z. H.; Shen, Y. R. Photoinduced Luminescence from the Noble-Metals and Its Enhancement on Roughened Surfaces. *Phys. Rev. B* **1986**, *33*, 7923–7936.
21. Sonnichsen, C.; Franzl, T.; Wilk, T.; von Plessen, G.; Feldmann, J.; Wilson, O.; Mulvaney, P. Drastic Reduction of Plasmon Damping in Gold Nanorods. *Phys. Rev. Lett.* **2002**, *88*, 077402-1.
22. Hu, M.; Novo, C.; Funston, A.; Wang, H. N.; Staleva, H.; Zou, S. L.; Mulvaney, P.; Xia, Y. N.; Hartland, G. V. Dark-Field Microscopy Studies of Single Metal Nanoparticles: Understanding the Factors that Influence the Linewidth of the Localized Surface Plasmon Resonance. *J. Mater. Chem.* **2008**, *18*, 1949–1960.
23. Knight, M. W.; Fan, J.; Capasso, F.; Halas, N. J. Influence of Excitation and Collection Geometry on the Dark Field

Spectra of Individual Plasmonic Nanostructures. *Opt. Express* **2010**, *18*, 2579–2587.
24. Duan, H.; Fernández-Domínguez, A. I.; Bosman, M.; Maier, S. A.; Yang, J. K. W. Nanoplasmonics: Classical down to the Nanometer Scale. *Nano Lett.* **2012**, *12*, 1683–1689.
25. Schuck, P. J.; Fromm, D. P.; Sundaramurthy, A.; Kino, G. S.; Moerner, W. E. Improving the Mismatch between Light and Nanoscale Objects with Gold Bowtie Nanoantennas. *Phys. Rev. Lett.* **2005**, *94*, 017402.
26. Wissert, M. D.; Ilin, K. S.; Siegel, M.; Lemmer, U.; Eisler, H.-J. Coupled Nanoantenna Plasmon Resonance Spectra from Two-Photon Laser Excitation. *Nano Lett.* **2010**, *10*, 4161–4165.
27. Rechberger, W.; Hohenau, A.; Leitner, A.; Krenn, J. R.; Lamprecht, B.; Aussenegg, F. R. Optical Properties of Two Interacting Gold Nanoparticles. *Opt. Commun.* **2003**, *220*, 137–141.
28. Lassiter, J. B.; Aizpurua, J.; Hernandez, L. I.; Brandl, D. W.; Romero, I.; Lal, S.; Hafner, J. H.; Nordlander, P.; Halas, N. J. Close Encounters between Two Nanoshells. *Nano Lett.* **2008**, *8*, 1212–1218.
29. Hohlfeld, J.; Wellershoff, S. S.; Güdde, J.; Conrad, U.; Jähnke, V.; Matthias, E. Electron and Lattice Dynamics Following Optical Excitation of Metals. *Chem. Phys.* **2000**, *251*, 237–258.
30. Hwang, Y.-N.; Jeong, D. H.; Shin, H. J.; Kim, D.; Jeoung, S. C.; Han, S. H.; Lee, J.-S.; Cho, G. Femtosecond Emission Studies on Gold Nanoparticles. *J. Phys. Chem. B* **2002**, *106*, 7581–7584.
31. Bigot, J. Y.; Halté, V.; Merle, J. C.; Daunois, A. Electron Dynamics in Metallic Nanoparticles. *Chem. Phys.* **2000**, *251*, 181–203.
32. Zheng, J.; Nicovich, P. R.; Dickson, R. M. Highly Fluorescent Noble-Metal Quantum Dots. *Annu. Rev. Phys. Chem.* **2007**, *58*, 409–431.
33. Nelayah, J.; Kociak, M.; Stephan, O.; Garcia de Abajo, F. J.; Tence, M.; Henrard, L.; Taverna, D.; Pastoriza-Santos, I.; Liz-Marzan, L. M.; Colliex, C. Mapping Surface Plasmons on a Single Metallic Nanoparticle. *Nat. Phys.* **2007**, *3*, 348–353.
34. Koh, A. L.; Fernández-Domínguez, A. I.; McComb, D. W.; Maier, S. A.; Yang, J. K. W. High-Resolution Mapping of Electron-Beam-Excited Plasmon Modes in Lithographically Defined Gold Nanostructures. *Nano Lett.* **2011**, *11*, 1323–1330.
35. Schaffer, B.; Hohenester, U.; Trugler, A.; Hofer, F. High-Resolution Surface Plasmon Imaging of Gold Nanoparticles by Energy-Filtered Transmission Electron Microscopy. *Phys. Rev. B* **2009**, *79*, 041401(R).
36. Frimmer, M.; Coenen, T.; Koenderink, A. F. Signature of a Fano Resonance in a Plasmonic Metamolecule's Local Density of Optical States. *Phys. Rev. Lett.* **2012**, *108*, 077404.
37. Hartland, G. V. Optical Studies of Dynamics in Noble Metal Nanostructures. *Chem. Rev.* **2011**, *111*, 3858–3887.